HHS Public Access

Author manuscript

J Proteome Res. Author manuscript; available in PMC 2016 March 22.

Published in final edited form as:

J Proteome Res. 2015 December 4; 14(12): 5306–5317. doi:10.1021/acs.jproteome.5b00802.

Multiplexed, Proteome-Wide Protein Expression Profiling: Yeast Deubiquitylating Enzyme Knockout Strains

Marta Isasa[†], **Christopher M. Rose**[†], **Suzanne Elsasser**[†], **José Navarrete-Perea**[‡], **Joao A. Paulo**[†], **Daniel J. Finley**[†], and **Steven P. Gygi**[*,†]

[†]Department of Cell Biology, Harvard Medical School, Boston, Massachusetts 02115, United States

[‡]National Autonomous University of Mexico, Av. Universidad 3000, Mexico City, District Federal 04510, Mexico

Abstract

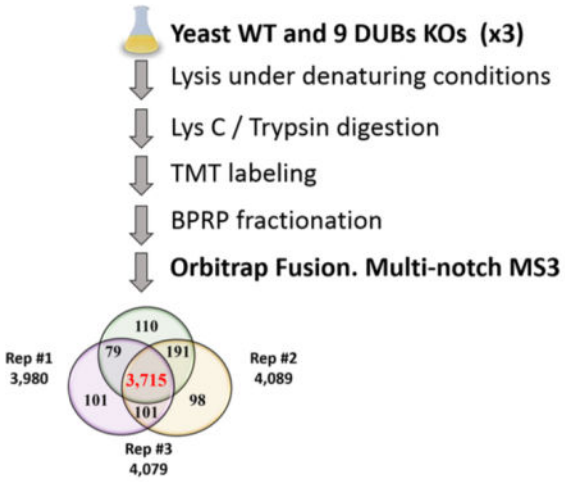

[*]Corresponding Author: steven_gygi@hms.harvard.edu.

Notes

The authors declare no competing financial interest.

ASSOCIATED CONTENT

Supporting Information

The Supporting Information is available free of charge on the ACS Publications website at DOI: 10.1021/acs.jproteo-me.5b00802.

Supplementary experimental procedures; yeast strains used in this study; sequence of the oligonucleotid primers used in the present study; number of peptide-spectrum matches as a function of the number of requirement-passing quantification filters; nonadjacent BPRP fractions reduce peptide redundancy in a large-scale analysis; deletion strains showed expected loss of deleted proteins; effect of DUB deletions in the ubiquitin signaling pathway; overview of the multiplexed quantitative proteomics analysis of Ubp3 overexpression; low protein abundances of the mitochondrial oxidative phosphorylation system in UBP3 KO are increased when Ubp3 is overexpressed; protein abundances of the quantified PHO-related genes in all 9 DUBs deletion strains; schematic of the inorganic phosphate pathway in yeast; increased ubiquitylation of Pho84 in UBP3 deletion strain compared to the other DUBs KOs (PDF)

Relative abundances of proteins quantified in triplicate in wild type and nine deubiquitylating enzyme deletion strains (XLSX)

Relative abundances of all proteins quantified in wild type, UBP3 KO, and Ubp3 OE triplicate strains (XLSX)

Characterizing a protein's function often requires a description of the cellular state in its absence. Multiplexing in mass spectrometry-based proteomics has now achieved the ability to globally measure protein expression levels in yeast from 10 cell states simultaneously. We applied this approach to quantify expression differences in wild type and nine deubiquitylating enzyme (DUB) knockout strains with the goal of creating "information networks" that might provide deeper, mechanistic insights into a protein's biological role. In total, more than 3700 proteins were quantified with high reproducibility across three biological replicates (30 samples in all). DUB mutants demonstrated different proteomics profiles, consistent with distinct roles for each family member. These included differences in total ubiquitin levels and specific chain linkages. Moreover, specific expression changes suggested novel functions for several DUB family members. For instance, the *ubp3*Δ mutant showed large expression changes for members of the cytochrome *C* oxidase complex, consistent with a role for Ubp3 in mitochondrial regulation. Several DUBs also showed broad expression changes for phosphate transporters as well as other components of the inorganic phosphate signaling pathway, suggesting a role for these DUBs in regulating phosphate metabolism. These data highlight the potential of multiplexed proteome-wide analyses for biological investigation and provide a framework for further study of the DUB family. Our methods are readily applicable to the entire collection of yeast deletion mutants and may help facilitate systematic analysis of yeast and other organisms.

Keywords

high-throughput proteomics; quantitative proteomics; isobaric labeling; TMT; Orbitrap Fusion; deubiquitinases; UBP3; ubiquitin; COX complex; inorganic phosphate pathway

INTRODUCTION

The completion of the yeast genome sequence in 1996 led to the development of tools enabling analysis of molecular components and interactions within eukaryotic cells. Chief among these tools is the yeast deletion collection, which contains one haploid strain of each mating type for every nonessential gene (4757 genes) and homozygous and heterozygous diploid strains for 5916 genes (including 1159 essential ones).[1] Major scientific contributions have arisen from the use of this collection including exhaustive phonotype screening studies,[2,3] generation of synthetic lethal mutants to investigate drug targets,[3,4] and identification of novel components of complex metabolic pathways.[2,5] To date, however, few studies have focused on proteome alterations incurred by the systematic deletion of genes.

Significant improvements in multiplexed quantitative proteomics have expanded the depth of proteome analysis, enabling near-comprehensive analyses of entire proteomes in a highly multiplexed format. Specifically, advances in isobaric labeling technologies (e.g., tandem mass tag; TMT) now support comparisons of up to 10 samples simultaneously using reporter ions that are well distinguished by high-resolution mass spectrometry.[6,7] Simultaneous analysis greatly reduces the impact of run-to-run reproducibility. Additionally, precursor ions from all 10 samples labeled with isobaric tags appear as a single peak in MS1 mass spectra, enhancing the quantification of peptides with low abundance. Previous studies have

demonstrated that isobaric labels exhibit reporter ion interference from coisolated precursors.[8–10] However, the introduction of MS3-based and synchronous precursor selection (SPS) methods restores quantitative accuracy[10] and greatly improves sensitivity,[11] respectively. The SPS-MS3 method was commercialized on Orbitrap Fusion mass spectrometers where MS2 and MS3 scans are parallelized, increasing data acquisition speed and enabling relative protein expression profiling from complex protein samples.

Ubiquitin-dependent signaling is modulated by proteases termed deubiquitylating enzymes (DUBs). The yeast genome encodes 20 DUBs. DUBs are tightly regulated in space and time and can act as both negative and positive regulators of the ubiquitin system in multiple cellular roles.[12] DUBs display specificity at several levels and discriminate: (i) between Ub and Ub-like proteins, (ii) among target proteins to which the Ub moiety is conjugated, and (iii) among different types of Ub linkage and chain structure.[12,13] Importantly, specificity is not governed by membership in particular DUB families. The ubiquitin-specific proteases (Ubp family) cleave ubiquitin from a range of substrates, while the Uch family (ubiquitin carboxy-terminal hydrolase) cleaves Ub from peptides and small adducts.[12] The ovarian tumor proteases (OTUs) encompass members with exquisite linkage specificity in mammalian cells,[14] but still little is known in yeast.

In this study, we sought to benchmark our multiplexing workflow for yeast proteome analysis by applying it to the analysis of nine DUB deletion strains. Herein, we demonstrate that replicate analyses of wild type and nine deletion strains for individual DUB deletions are reproducible with 4395 proteins quantified at least once and 3715 proteins quantified across all 30 samples. High reproducibility of biological replicates facilitated statistical analysis, confirming many known functions and enabling new discoveries for these undercharacterized DUBs. Specifically, we found a broad upregulation of the cytochrome *C* oxidase complex components upon *UBP3* deletion, suggesting a specific role of this DUB in the mitochondrial oxidative phosphorylation system. Moreover, members of the PHO-signaling pathway were strongly downregulated in *UBP3*, *UBP10*, and *OTU2* deletion strains but upregulated in *UBP15* and *OTU1* deletion strains, suggesting complementary roles in the absorption and maintenance of adequate cellular phosphate levels.

EXPERIMENTAL PROCEDURES

Media and Growth Conditions

Yeast were cultured at 30 °C with vigorous shaking. YPD medium (yeast extract/peptone/dextrose) and synthetic complete medium (SC) were prepared according to standard procedures.[15] Phosphate-rich medium consisted of 2% dextrose, 0.5% ammonium sulfate, 0.08% CSM (Complete Supplement Mixture; Sunrise, San Diego, CA), and 0.17% YNB (Yeast Nitrogen Base #1500; Sunrise, San Diego, CA). For the non-phosphate medium, the same reagents were used, but YNB without phosphate (Yeast Nitrogen Base #1532; Sunrise, San Diego, CA) was used. Transformations were performed with a standard lithium acetate method.

Harvest and Cell Lysis

Yeast cultures were pelleted at 1500 × *g*, washed twice with cold deionized water, and resuspended in a buffer containing 50 mM HEPES pH 8.2, 8 M urea, 50 mM NaCl, and protease inhibitors (complete mini, EDTA-free; Roche, Basel, Switzerland). Cells were lysed using the Mini-Beadbeater (Biospec, Bartlesville, OK) in microcentrifuge tubes containing 3 g of zirconia/silica beads (Research Products International, Mt. Prospect, IL) at maximum speed for three cycles of 60 s each, with 3 min pauses between cycles to avoid overheating of the lysates. Lysates were cleared by centrifugation at 11 200 × *g* for 10 min and were transferred to new tubes. Protein concentration was determined using the bicinchoninic acid (BCA) protein assay (Thermo Fisher Scientific, Waltham, MA).

Cysteine residues in the lysate were subjected to disulfide reduction with 5 mM tris(2-carboxyethyl)phosphine (TCEP) for 45 min at room temperature, then alkylated with 10 mM iodoacetamide for 30 min in the dark at room temperature. Excess of iodoacetamide was quenched with 15 mM dithiotreitol at room temperature for 15 min. Aliquots of 200 μg of protein were made and stored at −80 °C for future immunoblotting analysis.

Protein Digestion and TMT Labeling

Methanol–chloroform precipitation was performed prior to protease digestion. In brief, four volumes of neat methanol were added to each sample and vortexed, one volume chloroform was added to the sample and vortexed, and three volumes water was added to the sample and vortexed. The sample was centrifuged at 2000 × *g* for 15 min at room temperature and subsequently washed twice with 100% cold methanol prior to air-drying.

Samples were resuspended in 100 μL of 8 M urea, 50 mM HEPES (pH 8.2) buffer. Protein extracts were then diluted to 4 M urea with 50 mM HEPES (pH 8.2) and digested at room temperature for 3 h with endoproteinase Lys-C (Wako, Japan) at 5 ng/μL. The mixtures were then diluted to 1 M urea with 50 mM HEPES (pH 8.2), and trypsin was added at a 50:1 protein-to-protease ratio. The reaction was incubated overnight at 37 °C and stopped by acidification with TFA 0.4% (v/v) (pH < 2). Peptides were desalted using 50 mg tC18 SepPak solid-phase extraction cartridges (Waters, Milford, MA) and lyophilized. Desalted peptides were resuspended in 100 μL of 200 mM HEPES (pH 8.2). Peptide concentrations were determined using the microBCA assay (Thermo Fisher Scientific, Waltham, MA). One-hundred micrograms of peptides from each sample was labeled with TMT reagent. TMT reagents (0.8 mg) were dissolved in anhydrous acetonitrile (40 μL), of which 10 μL was added to the peptides along with 30 μL of acetonitrile (final acetonitrile concentration of approximately 30% (v/v)). The labeling reaction proceeded for 1 h at room temperature and then was quenched with hydroxylamine (Sigma, St. Louis, MO) to a final concentration of 0.3% (v/v). The TMT-labeled samples were mixed equally, vacuum centrifuged to near dryness, desalted using 200 mg solid-phase C18 extraction cartridge (Sep-Pak, Waters), and lyophilized.

Off-Line Basic pH Reversed-Phase (BPRP) Fractionation

The TMT-labeled peptide samples were fractionated using BPRP HPLC. We used an Agilent 1100 pump equipped with a degasser and a photodiode array (PDA) detector (set at

220 and 280 nm wavelength) from Thermo Fisher Scientific (Waltham, MA). Peptides were subjected to a 50 min linear gradient from 5% to 35% acetonitrile in 10 mM ammonium bicarbonate pH 8 at a flow rate of 0.8 mL/min over an Agilent 300 Extend C18 column (5 μm particles, 4.6 mm ID, and 220 mm in length). Beginning at 10 min of peptide elution, fractions were collected every 0.38 min into a total of 96 fractions, which were consolidated into 24, of which only 12 nonadjacent samples were analyzed. Samples were dried via vacuum centrifugation. Each eluted fraction was acidified with 1% formic acid and desalted using homemade StageTips,[16] dried via vacuum centrifugation, and reconstituted in 4% acetonitrile, 5% formic acid for LC–MS/MS analysis.

Liquid Chromatography and Tandem Mass Spectrometry

All mass spectrometry data were collected on an Orbitrap Fusion mass spectrometer (Thermo Fisher Scientific, San Jose, CA) coupled to a Proxeon EASY-nLC II liquid chromatography (LC) pump (Thermo Fisher Scientific). Peptides were eluted over a 75 μm inner diameter microcapillary column packed with ~0.5 cm of Magic C4 resin (5 μm, 100 Å, Michrom Bioresources) followed by ~30 cm of GP-18 resin (1.8 μm, 200 Å, Sepax, Newark, DE). For each analysis, we loaded ~1 μg total onto the column. Peptides were separated using a 2 h gradient of 6–26% acetonitrile in 0.125% formic acid at a flow rate of ~350 nL/min. The dynamics exclusion duration was set at 90 s, with a range in mass tolerance of ±7 ppm. Each analysis used the multinotch MS3-based TMT method[11] on an Orbitrap Fusion mass spectrometer. The scan sequence began with an MS1 spectrum (Orbitrap analysis; resolution 120 000; mass range 400–1400 *m*/*z*; automatic gain control (AGC) target 2 × 105; maximum injection time 100 ms). The 10 most-abundant MS1 ions of charge states 2–6 were fragmented, and multiple MS2 ions were selected using a TopSpeed of 2 s. MS2 analysis was composed of collision-induced dissociation (quadrupole ion trap analysis; AGC 4 × 103; normalized collision energy (NCE) 35; maximum injection time 150 ms). Following acquisition of each MS2 spectrum, we collected an MS3 spectrum as described in ref 11, in which multiple MS2 fragment ions are captured in the MS3 precursor population using isolation waveforms with multiple frequency notches. MS3 precursors were fragmented by high energy collision-induced dissociation (HCD) and analyzed using the Orbitrap (NCE 55; AGC 5 × 104; maximum injection time 150 ms, resolution was 60K at 400 Th).

Data Analysis

Instrument data files were processed using a SEQUEST-base in-house software pipeline.[17] Spectra were converted from *.raw* to mzXML using a modified version of ReadW.exe. Database searching included all predictive ORFs for entries from the yeast SGD (http://www.yeastgenome.org/download-data; downloaded March 12, 2014). This database was concatenated with a database composed of all protein sequences in the reversed order. Searches were performed using a 50 ppm precursor ion tolerance for total protein level analysis. The product ion tolerance was set to 0.9 Da. These wide mass tolerance windows were chosen to maximize sensitivity besides Sequest searches and linear discriminant analysis.[17,18] TMT tags on lysine residues and peptide N termini (+229.163 Da) and carbamidomethylation of cysteine residues (+57.021 Da) were set as static modifications,

while oxidation of methionine residues (+15.995 Da) was established as a variable modification.

Peptide-spectrum matches (PSMs) were adjusted to a 1% false discovery rate (FDR).[19] PSM filtering was performed using a linear discriminant analysis, as described previously,[17] while considering the following parameters: XCorr, ΔCn, missed cleavages, peptide length, charge state, and precursor mass accuracy. For TMT-based reporter ion quantitation, we extracted the signal-to-noise (S/N) ratio for each TMT channel and found the closest matching centroid to the expected mass of the TMT reporter ion. PSMs were identified, quantified, and collapsed to a 1% peptide FDR and then collapsed further to a final protein-level FDR of 1%. Moreover, for protein assembly, principles of parsimony were used to produce the smallest set of proteins necessary to account for all observed peptides.

Proteins were quantified by summing reporter ion counts across all matching PSMs using in-house software, as described previously.[17] Briefly, a 0.003 Th window around the theoretical *m*/*z* of each reporter ion (126, 126.1278 Th; 127N, 127.1249 Th; 127C, 127.1310 Th; 128N, 128.1283 Th; 128C, 128.1343 Th; 129N, 129.1316 Th; 129C, 129.1377 Th; 130N, 130.1349 Th; 130C, 130.1410 Th; 131, 1311 382 Th) was scanned for ions, and the maximum intensity nearest the theoretical *m*/*z* was used. PSMs with poor quality, MS3 spectra with more than nine TMT reporter ion channels missing, MS3 spectra with TMT reporter summed signal-to-noise ratio less than 387, or no MS3 spectra were excluded from quantitation[20] (Supplementary Figure 1). The mass spectrometry proteomics data have been deposited to the ProteomeXchange Consortium[21] via the PRIDE partner repository with the data set identifier PXD003033. Protein quantitation values were exported for further analysis in Excel, Perseus 1.5.2.4, MeV v4.8, or R. Each reporter ion channel was summed across all quantified proteins and normalized assuming equal protein loading of all 10 samples.

Pho4-GFP Colocalization Assays

Strains yMIC34, yMIC35, yMIC36, and yMIC37 (Table S1) were used to monitor the cellular colocalization of Pho4-GFP. The activity of Pho80/Pho85^{F82G} was inhibited as reported in Carroll et al.[22] Cells were normally grown overnight in YPD and diluted up to an initial OD_{600} of ~0.1 in 5 mL of YPD. Inducible overexpression of Ubp3 was performed as described in the Supporting Information. At an approximate OD_{600} of 0.8, cells were fixed for 30 min at 30 °C by adding 4% final concentration of formaldehyde (Electron Microscopy Sciences, Hatfield, PA), harvested by centrifugation, and washed three times with 50 mM sodium citrate (pH 7) buffer. Cells were concentrated at ~1E7 cells per mL and gently vortexed to resuspend and declump. Three microliters were spotted onto poly lysine slides (NeuVitro, Vancouver, WA), dried at room temperature for 10 min, and 4 μL of VECTASHIELD with DAPI (Vector Laboratories, Burlingame, CA) was added. Coverslips were incubated for 15 min at room temperature in dark and were sealed with clear nail polish prior to image analysis.

All images were collected with a Nikon A1R point scanning confocal on a Nikon Ti inverted microscope equipped with a 100× Plan Apo VC NA 1.4 objective lens (0.249 μm per pixel). Pho4-GFP fluorescence was excited with the 488 nm laser line, and emission light was

selected with a 525/50m filter (Chroma). For DAPI fluorescence, a 404 nm laser and a 450/50m emission filter (Chroma) was used. Images were acquired with NIS Elements software (Nikon Instruments). Images were analyzed with Fiji, and the Pearson's R value was set for all the analyzed samples.

RESULTS AND DISCUSSION

Proteomic Analysis of Nine DUB Deletion Strains in Saccharomyces cerevisiae

Ubiquitylation often marks proteins for degradation, altering protein levels in the cell in a manner that cannot be measured by large-scale RNA experiments. DUBs are important for proper maintenance of cellular protein levels and signaling due to their ability to remove ubiquitin from substrates as well as cleave pro-ubiquitin proteins to their final, active form. To probe proteome alterations upon their deletion, we performed multiplexed proteome analysis using the TMT10 workflow (Figure 1A). Deletion strains were chosen from two DUB families: ubiquitin specific proteases (*UBP3*, *DOA4*, *UBP6*, *UBP8*, *UBP10*, *UBP14*, and *UBP15*) and ovarian-tumor proteases (*OTU1* and *OTU2*). Before our proteomics analysis was started, we confirmed correct replacement of the target gene with the KanMX cassette by the appearance of PCR products (data not shown). Despite their importance in protein homeostasis, deletion of these nine DUBs does not cause severe growth retardation compared to wild type (Figure 1B). These results are in agreement with previous studies on cell viability of DUB deletions in yeast.[23,24]

To ensure results were representative of deletions in a specific DUB, cultures were started from a mixed patch of cells rather than from a single colony. With this approach, we minimized the effects of random mutations in the genome as well as possible retentions of a wild type copy because of aneuploidy.[25,26] Proteins were then extracted, digested with a combination of LysC and trypsin, TMT labeled, separated by basic pH-reversed phase (BPRP) fractionation, and finally analyzed by mass spectrometry. To reduce peptide redundancy, a total of 12 nonadjacent offline fractions were analyzed over 2 h gradients, constituting 24 h of instrument time per biological replicate (Supplementary Figure 2). With this method, we quantified 3980, 4089, and 4079 proteins in three replicate 10-plex analyses in just 3 days of instrument time (Figure 1C). Impressively, 4395 proteins were quantified in at least one 10-plex replicate, and 3715 proteins (Supplementary Table 3), ~ 75% of protein coding ORFs, were quantified across all three replicates, yielding 30 quantitative measurements.

Previously, we and others have demonstrated that measurements made with isobaric labels can suffer from ratio compression due to coisolated precursor interference.[8–10] This phenomenon can cause large fold changes to appear much smaller (2–3-fold). To address this, we introduced an MS3 method that dissociates a precursor by CID and then simultaneously isolates multiple fragment ions that are further dissociated by HCD to produce reporter ions and enable quantitative measurements with little or no interference. Using this method, we generally see large fold changes (~10-fold) for proteins that have been knocked out (Figure 1E). The impact of residual precursor interference is more apparent when analyzing single peptide measurements (Supplementary Figure 3A). For instance, while almost all of the peptides for Ubp6 demonstrated a large fold change, the

peptide, FDPSSENVMTPR, still exhibited some precursor interference as signal was present in the KO channel (Supplementary Figure 3B). Inspection of all peptides from deleted proteins showed that nearly all reported ratios indicated the protein was deleted. It is important to note that the large fold change of these peptides is aided by the use of the SPS-MS3 method, as precursor interference would greatly truncate these measurements.[11]

Proteomic Changes in Ubiquitin Signaling Pathway Following DUB Deletion

Ubiquitin (Ub) is a 76-amino acid protein that serves both to target proteins for proteasomal degradation and as a dynamic signaling agent regulating the stability, activity, or subcellular localization of the target protein (Figure 2). Ub itself can be modified through any of seven internal lysine residues or its amino-terminal methionine, creating chains that have various functions within the cell (Figure 2A). The primary role of DUBs is to remove Ub from substrates, so deletion of DUBs genes could potentially have drastic effects on the overall cellular pool of Ub. Ub conjugate levels were elevated within the cell upon deletion of *UBP3*, but they trended lower for all other DUBs (Figure 2B). Importantly, the *ubp6*Δ strain shows a significant decrease in Ub conjugates, an effect that is recapitulated through Western blot analysis (Figure 2C). Ubp6 regenerates Ub from Ub conjugates degraded by the proteasome.[27] Our data suggest that in the absence of Ubp6, the proteasome destroys Ub along with its substrates resulting in a smaller Ub pool.[28]

Ub–Ub covalent linkages are a common phenomenon in the cell such that ubiquitylated ubiquitin peptides can be identified without previous enrichment.[29] A database search for peptides bearing the diglycine remnant present on ubiquitylated peptides after trypsin digestion returned two ubiquitylation sites on Ub itself, Lys^{48}, and Lys^{63} (Figure 2D). Ubiquitylation of Lys^{48} is involved in targeting the substrate to the proteasome, and increased levels of cellular Lys^{48} lead to protein degradation. Specifically, ubiquitylation of Lys^{48} increases in *ubp3*Δ and is potentially responsible for the increase of ubiquitin conjugates. Likewise, the decrease of Lys^{48} ubiquitylation in the *ubp6*Δ strain is caused by an increased proteasomal activity,[27,30] which potentially explains the decrease in the level of overall Ub for this strain (Figure 2D, top panel). Ubiquitylation of Lys^{63} is involved in endocytosis, DNA damage response, and signaling processes within the cell. Interestingly, Lys^{63} ubiquitylation increases in *doa4*Δ but decreases in *ubp8*Δ strain (Figure 2D, bottom panel). Doa4 functions primarily in membrane protein trafficking,[31] and an increase of Lys^{63} ubiquitylation in *doa4*Δ could indicate its preferred affinity to cleave Lys^{63}-specifc linkages. These results indicate that large-scale analysis of the ubiquitylome might help demonstrate specificity of DUBs.

Yeast encodes for ~140 genes involved in ubiquitin biology,[12] and this study returned expression levels for 112. Minor changes were detected in the whole Ub-signaling pathway. However, the deletion of *UBP3* caused an increase in many of the E2 ubiquitin conjugating enzymes such as Ubc1, Ubc4, Ubc7, and Ubc13 while also causing a decrease in the unique E1 ubiquitin activating enzyme Uba1 (Supplementary Table 3; Supplementary Figure 4, insets).

Effect of Individual DUB Knockouts on Protein Abundances

Reproducibility of proteomic measurements is essential for the analysis of small, but significant changes in protein expression (Figure 3; Supplementary Table 3). Hierarchical clustering and principal component analysis demonstrated that biological replicates clustered tightly for each DUB KO strain (Figure 3A,B). Interestingly, the effects of deleting *OTU2* and *UBP10* appeared similar as these two proteins clustered by both types of analysis (Figure 3A,B). To determine the number of proteins that significantly and specifically changed upon deletion, we performed an ANOVA for each protein (p-value <0.01, Benjamini–Hochberg correction) followed by Tukey's posthoc test (p-value <0.01 in ≥ 5 comparisons) with a fold-change threshold of 1.5 (Figure 3C). A previous study revealed that the largest number of protein changes occurred after deletion of *UBP3*, suggesting as much as 30% of the proteome is changing in the *ubp3*Δ strain.[24] Our analysis confirmed that the largest alteration in protein expression occurred with *UBP3* KO, followed by *UBP10* and *OTU2* deletion strains where >100 proteins were significantly altered. Interestingly, the effect of the deletion of these individual DUBs on yeast proteome is apparently not related to their cellular absolute abundance;[32] that is, Otu2 (2822 molecules/cell)[32] is >5-fold more abundant than Ubp10 (521 molecules/cell),[32] but *ubp10*Δ has a major effect on the yeast proteome (Figure 3C).

All DUB deletion strains exhibited significant protein alterations. To determine which pathways were affected, significantly changing proteins (ANOVA, $p < 0.01$ with Benjamini–Hochberg correction) were tested for enrichment of GO and KEGG pathway annotations using DAVID ($p < 0.01$ with Benjamini–Hochberg correction). A subset of significantly altered protein abundances is plotted along with the fold-change of the deleted protein in Figure 4. The deletion strain with the largest number of changes, *ubp3*Δ, appeared to mainly exhibit alterations in the phosphate pathway, iron–iron binding, and cellular respiration (Figure 4A). In general, proteins related to mitochondrial biology were upregulated upon deletion of *UBP3*, which corroborates recent reports of Ubp3 as a negative regulator of mitophagy.[33] *DOA4* deletion has been linked to changes in the vacuolar sorting pathway (VSP), specifically altering endocytosis and vacuolar targeting of yeast membrane proteins.[34] We found that Doa4 appeared to be important in amine transport with many proteins (e.g., Bap3, Mup1, Can1, etc.) significantly increasing their abundance by >2.5-fold only in the *doa4*Δ mutant (Figure 4B). *UBP15* deletion strains exhibited large increases in proteins related to methionine synthesis and glucose metabolism (Figure 4G). Previous studies have demonstrated that *ubp15*Δ causes upregulation of genes involved in metabolism and alters the sulfur amino acid, methionine, and arginine biosynthetic pathway.[35] Recently, knockdown (KD) of OTUB2, the human homologue of Otu2, has been shown to enhance RNF8-mediated ubiquitination in the early phase of DNA double strand break response, suppressing homologous recombination, but promoting fast doubles strand break repair.[36] Interestingly, both the *OTU1* and *OTU2* deletion strains demonstrated significant upregulation in the DNA repair pathway, mirroring the role of the human homologue. We found that Msh2, Msh3, and Msh6 were significantly upregulated in both *otu1*Δ and *otu2*Δ strains, while many more proteins involved in the DNA repair pathway (e.g., Pol3, Sin3, Tfb2, Rdh54, Rad5, Scc2, and Rsc20) were only increasing significantly in the *otu2*Δ mutant (Figure 4H,I). These results demonstrate that DUB deletions often offered unique proteome

alterations such as the alterations in cytochrome *C* oxidase (COX) complex upon *UBP3* deletion and the differing alterations in the PHO pathway.

Specific Role of UBP3 in the Cytochrome *C* Oxidase Complex

Our proteomic analysis indicated a broad upregulation of the COX components in *ubp3*Δ (Figure 4A; Supplementary Table 3). COX is the terminal electron acceptor in the mitochondrial respiratory chain, and specific deficiencies in COX account for a significant proportion of known mitochondrial defects.[37] The functional yeast COX holoenzyme consists of 11 subunits: three form the catalytic core of the complex (Cox1, Cox2, and Cox3) and are encoded by the mitochondrial DNA, and the remaining eight are encoded in the nuclear genome.[38] In addition, there are the so-called assembly factors that are involved in the COX assembly process.[38] Our data set enabled us to quantify the vast majority of the COX subunits and assembly factors (>80%) in yeast across all 30 samples. Strikingly, the most subunits showed a significant increase in *ubp3*Δ when compared to the rest of KOs strains (Figure 5A). Because of unique peptide detection, our method could differentiate and quantify the two distinct forms of COX subunit V, Cox5a and Cox5b, both upregulated in *ubp3*Δ by 3.5-fold (Figure 5B).

To determine whether this increase in COX subunits was both Ubp3 specific and physiologically relevant, we employed two strategies. First, to ascertain Ubp3 specificity, we analyzed the effect of Ubp3 overexpression. Deletion of *UBP3* increased expression levels among members of the COX complex. We reasoned that Ubp3 overexpression should return opposite patterns. To address this question, we employed a conditional induction system that used the chimeric transcriptional activator $Zif268_4$.ER.VP16 (Z_4EV). Upon addition of the hormone, β-estradiol, cytoplasmatic Z_4EV translocates to the nucleus and activates transcription of the target protein that has been positioned downstream of the non-native promoter, resulting in rapid and specific induction[39] (Supplementary Tables 1 and 2). We then performed an additional multiplexed quantitative proteomics experiment in which triplicates of WT, *UBP3* KO, and hormone-induced Ubp3-Z_4EV (Ubp3 OE) were simultaneously compared (Supplementary Figure 5). Overall, we quantified >4300 proteins across all nine samples (Supplementary Table 4), including the vast majority of the COX-related components. Ubp3 was induced by >7-fold upon hormone induction, sufficient to drop the expression of the COX complex back to Ubp3 endogenous levels (Figure 5C, Supplementary Figure 6A). Importantly, the fold changes of the COX-related proteins of *ubp3*Δ with respect to WT were similar and statistically significant in both proteomic data sets, demonstrating the quantitative precision of our results (Supplementary Figure 6B). These data provide evidence for a novel function of Ubp3 in maintaining the energy balance of the cell and support its role in mitophagy regulation.[33]

Second, to determine if increased expression of COX subunits was physiologically relevant, the growth ability of all strains grown under respiratory stress was tested. Functional mitochondria are required for cells to utilize the non-fermentable carbon source glycerol as the sole energy source.[40] Mitochondria convert glycerol in dihidroxyacetone phosphate (DHAP), which in turn is used as a substrate for multiple energy producing pathways. Therefore, mitochondrial mutants will grow poorly in glycerol conditions. The fact that

*ubp3*Δ is slightly more resistant to YPGlycerol media (Figure 5D) suggests that Ubp3 altered mitochondrial biology in such a way that the mitochondria were better suited to convert glycerol to DHAP, providing cells with a growth advantage.[41]

DUB Knockouts Impact on the Inorganic Phosphate Pathway

The large scale survey presented here revealed striking expression differences within the inorganic phosphate pathway in response to DUB deletions (Figure 4; Supplementary Table 3). Inorganic phosphate (Pi) is indispensable for survival of all living organisms. Budding yeast has evolved a phosphate (PHO) responsive signaling pathway to monitor cytoplasmatic levels of phosphate under scarce phosphate conditions.[42] The PHO pathway entails three main components: (i) a membrane transporter system comprising low- and high-affinity phosphate transporters, (ii) polyphosphates, and (iii) the PHO core signaling cascade.[43] Of the 28 PHO-related genes, data from 24 were quantified across all 30 samples. All low-affinity phosphate transporters were strongly downregulated in *UBP3*, *UBP10*, and *OTU2* deletion strains, while the high-affinity transporters remained constant. Similar patterns were observed for some of the phosphatases (Pho5) or kinases (Pho81) of the core signaling cascade. Interestingly, genes with reduced expression in these three mutants were significantly upregulated in *ubp15*Δ and *otu1*Δ, suggesting that multiple members of the DUB family are involved in cellular phosphate homeostasis (Figures 4 and 6A; Supplementary Figure 7). Moreover, Ubp3 overexpression recapitulated protein abundances of most of the PHO-related genes (Figure 6B; Supplementary Table 4), indicating a key role of Ubp3 in phosphate homeostasis. We sought to verify these proteomics results using conventional immunoblotting techniques. Consistent with the proteomic data, levels of C-terminally FLAG tagged Pho5 and Pho84 showed a drastic reduction of expression in *UBP3*, *UBP10*, and *OTU2* KOs (Figure 6C).

As a result of the PHO signaling pathway, expression of many PHO genes is suppressed under high-phosphate conditions and induced under low-phosphate conditions (Supplementary Figure 8), including Pho5 and Pho84.[44] We monitored expression of Pho5 and Pho84 in strains cultivated in high- and nonphosphate media. In rich phosphate media, both Pho5 and Pho84 were strongly downregulated in *UBP3*, *UBP10*, and *OTU2* deletion strains, but they were induced upon Ubp3 overexpression and in *ubp15*Δ, mimicking data collected in YPD, considered medium-phosphate media. In nonphosphate conditions WT, *ubp10*Δ, *otu2*Δ and *ubp15*Δ strains demonstrate the expected induction of Pho5 and Pho84, but mutants, deletion or overexpression of *UBP3*, were not able to trigger these two PHO-related genes (Figure 6D). Moreover, a search for the diglycine remnant peptides in our proteomics data revealed an increase of ubiquitylated Pho84 at Lys^{297} in *ubp3*Δ mutant (Supplementary Figure 9), suggesting a role of Ubp3 in the Pho84 deubiquitylation reaction. We further validated the role of Ubp3 in the PHO signaling pathway by monitoring the cellular localization of the transcription factor Pho4 in rich-media-grown strains. The Pho80/Pho85 kinase complex regulates the phosphate starvation response by controlling the activity and localization of Pho4, which activates transcription of genes such as Pho5.[45,46] We used the chemical inhibition of the $Pho85^{F82G}$ mutant as a benchmark for Pho4 GFP-tagged cellular localization in both *ubp3*Δ and Ubp3 overexpression mutants so that when $Pho85^{F82G}$ is inhibited, Pho4 is retained in the nucleus.[47] We found that the inducible

overexpression of Ubp3 targeted the Pho4 transcription factor to the nucleus. Analysis of ~100 cells per strain allowed us to calculate the Pearson correlation of Pho4-GFP localization under the five investigated strains. Upon Ubp3 induction, its correlation value rose when compared to WT or *UBP3* KO cells but remained below our positive control (Figure 6E). Although further molecular validation is required to fully understand the function of DUBs in phosphate metabolism, data presented here clearly illustrate the power and applicability of multiplexed proteomics to identify novel roles within members of the same enzymatic family.

CONCLUSIONS

In summary, our data highlight the use of higher order TMT-based multiplexing to interrogate the global proteomes of multiple deletion strains in an unbiased manner toward discovering potential functional alterations. Further bioinformatic analysis of these data may yield insights into the mechanisms by these DUBs. Future experiments may also extend the strategy that we have outlined herein. This versatile strategy can be applied to virtually any organism, organs, or disease models, making it a powerful multiplexing method. Among the advantages of our TMT10-plex strategy used herein is overcoming the need for expensive metabolic labeling and the ability to apply this technique beyond yeast and cultured cells to any sample including human tissue and fluids.[48] Future technological developments will likely generate new reagents permitting an even higher degree of multiplexing. Upon the introduction of such higher-plexed isobaric labeling, a greater number of replicates or conditions could be analyzed in a single experiment potentially enabling the quantitative analysis of alterations across the full yeast proteome.

Supplementary Material

Refer to Web version on PubMed Central for supplementary material.

Acknowledgments

This work was supported by a grant from the NIH (GM67945) to S.P.G. We thank the Nikon Imaging Center at Harvard Medical School and Tiao Xie from the Image and Data Analysis Core of Harvard Medical School for help with colocalization analysis in Fiji.

ABBREVIATIONS

AGC	automatic gain control
BCA	bicinchoninic acid
BPRP	basic pH reverse-phase
COX	cytochrome *C* oxidase
DUB	deubiquitylating enzyme
FDR	false discovery rate
HCD	high energy collision-induced dissociation

KO	knockout
KD	knockdown
LC	liquid chromatography
NCE	normalized collision energy
OTU	ovarian tumor protease
PDA	photodiode array
PHO	phosphate responsive signaling pathway
PSM	peptide-spectrum matches
SC	synthetic complete
S/N	signal-to-noise
SPS	synchronous precursor selection
TCEP	tris(2-carboxyethyl)phosphine
TMT	tandem mass tag
Ub	Ubiquitin
UBP3 OE	hormone-induced UBP3-Z_4EV
VSP	vacuolar sorting pathway
YNB	yeast nitrogen base

References

1. Winzeler EA, Shoemaker DD, Astromoff A, Liang H, Anderson K, Andre B, Bangham R, Benito R, Boeke JD, Bussey H, Chu AM, Connelly C, Davis K, Dietrich F, Dow SW, El Bakkoury M, Foury F, Friend SH, Gentalen E, Giaever G, Hegemann JH, Jones T, Laub M, Liao H, Liebundguth N, Lockhart DJ, Lucau-Danila A, Lussier M, M'Rabet N, Menard P, Mittmann M, Pai C, Rebischung C, Revuelta JL, Riles L, Roberts CJ, Ross-MacDonald P, Scherens B, Snyder M, Sookhai-Mahadeo S, Storms RK, Veronneau S, Voet M, Volckaert G, Ward TR, Wysocki R, Yen GS, Yu K, Zimmermann K, Philippsen P, Johnston M, Davis RW. Functional characterization of the S. cerevisiae genome by gene deletion and parallel analysis. Science. 1999; 285(5429):901–6. [PubMed: 10436161]
2. Steinmetz LM, Scharfe C, Deutschbauer AM, Mokranjac D, Herman ZS, Jones T, Chu AM, Giaever G, Prokisch H, Oefner PJ, Davis RW. Systematic screen for human disease genes in yeast. Nat Genet. 2002; 31(4):400–4. [PubMed: 12134146]
3. Giaever G, Chu AM, Ni L, Connelly C, Riles L, Veronneau S, Dow S, Lucau-Danila A, Anderson K, Andre B, Arkin AP, Astromoff A, El-Bakkoury M, Bangham R, Benito R, Brachat S, Campanaro S, Curtiss M, Davis K, Deutschbauer A, Entian KD, Flaherty P, Foury F, Garfinkel DJ, Gerstein M, Gotte D, Guldener U, Hegemann JH, Hempel S, Herman Z, Jaramillo DF, Kelly DE, Kelly SL, Kotter P, LaBonte D, Lamb DC, Lan N, Liang H, Liao H, Liu L, Luo C, Lussier M, Mao R, Menard P, Ooi SL, Revuelta JL, Roberts CJ, Rose M, Ross-Macdonald P, Scherens B, Schimmack G, Shafer B, Shoemaker DD, Sookhai-Mahadeo S, Storms RK, Strathern JN, Valle G, Voet M, Volckaert G, Wang CY, Ward TR, Wilhelmy J, Winzeler EA, Yang Y, Yen G, Youngman E, Yu K, Bussey H, Boeke JD, Snyder M, Philippsen P, Davis RW, Johnston M. Functional profiling of the Saccharomyces cerevisiae genome. Nature. 2002; 418(6896):387–91. [PubMed: 12140549]

4. Blackburn AS, Avery SV. Genome-wide screening of Saccharomyces cerevisiae to identify genes required for antibiotic insusceptibility of eukaryotes. Antimicrob Agents Chemother. 2003; 47(2): 676–81. [PubMed: 12543677]

5. Kachroo AH, Laurent JM, Yellman CM, Meyer AG, Wilke CO, Marcotte EM. Evolution. Systematic humanization of yeast genes reveals conserved functions and genetic modularity. Science. 2015; 348(6237):921–5. [PubMed: 25999509]

6. Paulo JA, Gygi SP. A comprehensive proteomic and phosphoproteomic analysis of yeast deletion mutants of 14–3-3 orthologs and associated effects of rapamycin. Proteomics. 2015; 15(2–3):474–86. [PubMed: 25315811]

7. Murphy JP, Stepanova E, Everley RA, Paulo JA, Gygi SP. Comprehensive temporal protein dynamics during the diauxic shift in Saccharomyces cerevisiae. Mol Cell Proteomics. 2015; 14:2454–65. [PubMed: 26077900]

8. Wenger CD, Lee MV, Hebert AS, McAlister GC, Phanstiel DH, Westphall MS, Coon JJ. Gas-phase purification enables accurate, multiplexed proteome quantification with isobaric tagging. Nat Methods. 2011; 8(11):933–5. [PubMed: 21963608]

9. Werner T, Sweetman G, Savitski MF, Mathieson T, Bantscheff M, Savitski MM. Ion coalescence of neutron encoded TMT 10-plex reporter ions. Anal Chem. 2014; 86(7):3594–601. [PubMed: 24579773]

10. Ting L, Rad R, Gygi SP, Haas W. MS3 eliminates ratio distortion in isobaric multiplexed quantitative proteomics. Nat Methods. 2011; 8(11):937–40. [PubMed: 21963607]

11. McAlister GC, Nusinow DP, Jedrychowski MP, Wuhr M, Huttlin EL, Erickson BK, Rad R, Haas W, Gygi SP. MultiNotch MS3 enables accurate, sensitive, and multiplexed detection of differential expression across cancer cell line proteomes. Anal Chem. 2014; 86(14):7150–8. [PubMed: 24927332]

12. Finley D, Ulrich HD, Sommer T, Kaiser P. The ubiquitin-proteasome system of Saccharomyces cerevisiae. Genetics. 2012; 192(2):319–60. [PubMed: 23028185]

13. Komander D, Clague MJ, Urbe S. Breaking the chains: structure and function of the deubiquitinases. Nat Rev Mol Cell Biol. 2009; 10(8):550–63. [PubMed: 19626045]

14. Kulathu Y, Komander D. Atypical ubiquitylation - the unexplored world of polyubiquitin beyond Lys48 and Lys63 linkages. Nat Rev Mol Cell Biol. 2012; 13(8):508–23. [PubMed: 22820888]

15. Sherman F. Getting started with yeast. Methods Enzymol. 1991; 194:3–21. [PubMed: 2005794]

16. Rappsilber J, Ishihama Y, Mann M. Stop and go extraction tips for matrix-assisted laser desorption/ionization, nanoelectrospray, and LC/MS sample pretreatment in proteomics. Anal Chem. 2003; 75(3):663–70. [PubMed: 12585499]

17. Huttlin EL, Jedrychowski MP, Elias JE, Goswami T, Rad R, Beausoleil Sa, Villen J, Haas W, Sowa ME, Gygi SP. A tissue-specific atlas of mouse protein phosphorylation and expression. Cell. 2010; 143:1174–89. [PubMed: 21183079]

18. Beausoleil SA, Villen J, Gerber SA, Rush J, Gygi SP. A probability-based approach for high-throughput protein phosphorylation analysis and site localization. Nat Biotechnol. 2006; 24(10): 1285–92. [PubMed: 16964243]

19. Elias JE, Gygi SP. Target-decoy search strategy for increased confidence in large-scale protein identifications by mass spectrometry. Nat Methods. 2007; 4(3):207–14. [PubMed: 17327847]

20. McAlister GC, Huttlin EL, Haas W, Ting L, Jedrychowski MP, Rogers JC, Kuhn K, Pike I, Grothe RA, Blethrow JD, Gygi SP. Increasing the multiplexing capacity of TMTs using reporter ion isotopologues with isobaric masses. Anal Chem. 2012; 84(17):7469–78. [PubMed: 22880955]

21. Vizcaino JA, Deutsch EW, Wang R, Csordas A, Reisinger F, Rios D, Dianes JA, Sun Z, Farrah T, Bandeira N, Binz PA, Xenarios I, Eisenacher M, Mayer G, Gatto L, Campos A, Chalkley RJ, Kraus HJ, Albar JP, Martinez-Bartolome S, Apweiler R, Omenn GS, Martens L, Jones AR, Hermjakob H. ProteomeXchange provides globally coordinated proteomics data submission and dissemination. Nat Biotechnol. 2014; 32(3):223–6. [PubMed: 24727771]

22. Carroll, aS; Bishop, aC; DeRisi, JL.; Shokat, KM.; O'Shea, EK. Chemical inhibition of the Pho85 cyclin-dependent kinase reveals a role in the environmental stress response. Proc Natl Acad Sci U S A. 2001; 98:12578–83. [PubMed: 11675494]

23. Amerik AY, Li SJ, Hochstrasser M. Analysis of the deubiquitinating enzymes of the yeast Saccharomyces cerevisiae. Biol Chem. 2000; 381(9–10):981–92. [PubMed: 11076031]
24. Poulsen JW, Madsen CT, Young C, Kelstrup CD, Grell HC, Henriksen P, Juhl-Jensen L, Nielsen ML. Comprehensive profiling of proteome changes upon sequential deletion of deubiquitylating enzymes. J Proteomics. 2012; 75(13):3886–97. [PubMed: 22634085]
25. Grunenfelder B, Winzeler EA. Treasures and traps in genome-wide data sets: case examples from yeast. Nat Rev Genet. 2002; 3(9):653–61. [PubMed: 12209140]
26. Teng X, Dayhoff-Brannigan M, Cheng WC, Gilbert CE, Sing CN, Diny NL, Wheelan SJ, Dunham MJ, Boeke JD, Pineda FJ, Hardwick JM. Genome-wide consequences of deleting any single gene. Mol Cell. 2013; 52(4):485–94. [PubMed: 24211263]
27. Hanna J, Hathaway NA, Tone Y, Crosas B, Elsasser S, Kirkpatrick DS, Leggett DS, Gygi SP, King RW, Finley D. Deubiquitinating enzyme Ubp6 functions noncatalytically to delay proteasomal degradation. Cell. 2006; 127(1):99–111. [PubMed: 17018280]
28. Leggett DS, Hanna J, Borodovsky A, Crosas B, Schmidt M, Baker RT, Walz T, Ploegh H, Finley D. Multiple associated proteins regulate proteasome structure and function. Mol Cell. 2002; 10(3): 495–507. [PubMed: 12408819]
29. Kirkpatrick DS, Hathaway NA, Hanna J, Elsasser S, Rush J, Finley D, King RW, Gygi SP. Quantitative analysis of in vitro ubiquitinated cyclin B1 reveals complex chain topology. Nat Cell Biol. 2006; 8(7):700–10. [PubMed: 16799550]
30. Lee MJ, Lee BH, Hanna J, King RW, Finley D. Trimming of ubiquitin chains by proteasome-associated deubiquitinating enzymes. Mol Cell Proteomics. 2011; 10(5):R110.003871. [PubMed: 20823120]
31. Amerik A, Sindhi N, Hochstrasser M. A conserved late endosome-targeting signal required for Doa4 deubiquitylating enzyme function. J Cell Biol. 2006; 175(5):825–35. [PubMed: 17145966]
32. Kulak NA, Pichler G, Paron I, Nagaraj N, Mann M. Minimal, encapsulated proteomic-sample processing applied to copy-number estimation in eukaryotic cells. Nat Methods. 2014; 11(3):319–24. [PubMed: 24487582]
33. Muller M, Kotter P, Behrendt C, Walter E, Scheckhuber CQ, Entian KD, Reichert AS. Synthetic quantitative array technology identifies the Ubp3-Bre5 deubiquitinase complex as a negative regulator of mitophagy. Cell Rep. 2015; 10(7):1215–25. [PubMed: 25704822]
34. Amerik AY, Nowak J, Swaminathan S, Hochstrasser M. The Doa4 deubiquitinating enzyme is functionally linked to the vacuolar protein-sorting and endocytic pathways. Molecular biology of the cell. 2000; 11(10):3365–80. [PubMed: 11029042]
35. Benschop JJ, Brabers N, van Leenen D, Bakker LV, van Deutekom HW, van Berkum NL, Apweiler E, Lijnzaad P, Holstege FC, Kemmeren P. A consensus of core protein complex compositions for Saccharomyces cerevisiae. Mol Cell. 2010; 38(6):916–28. [PubMed: 20620961]
36. Kato K, Nakajima K, Ui A, Muto-Terao Y, Ogiwara H, Nakada S. Fine-tuning of DNA damage-dependent ubiquitination by OTUB2 supports the DNA repair pathway choice. Mol Cell. 2014; 53(4):617–30. [PubMed: 24560272]
37. Rich PR, Marechal A. The mitochondrial respiratory chain. Essays Biochem. 2010; 47:1–23. [PubMed: 20533897]
38. Soto IC, Fontanesi F, Liu J, Barrientos A. Biogenesis and assembly of eukaryotic cytochrome c oxidase catalytic core. Biochim Biophys Acta, Bioenerg. 2012; 1817(6):883–97.
39. McIsaac RS, Oakes BL, Wang X, Dummit KA, Botstein D, Noyes MB. Synthetic gene expression perturbation systems with rapid, tunable, single-gene specificity in yeast. Nucleic Acids Res. 2013; 41(4):e57. [PubMed: 23275543]
40. van Dijken JP, Scheffers WA. Redox balances in the metabolism of sugars by yeasts. FEMS Microbiol Lett. 1986; 32(3–4):199–224.
41. Yoshida S, Yokoyama A. Identification and characterization of genes related to the production of organic acids in yeast. J Biosci Bioeng. 2012; 113(5):556–61. [PubMed: 22277779]
42. Wykoff DD, O'Shea EK. Phosphate transport and sensing in Saccharomyces cerevisiae. Genetics. 2001; 159(4):1491–9. [PubMed: 11779791]
43. Lenburg ME, O'Shea EK. Signaling phosphate starvation. Trends Biochem Sci. 1996; 21(10):383–7. [PubMed: 8918192]

44. Huang S, O'Shea EK. A systematic high-throughput screen of a yeast deletion collection for mutants defective in PHO5 regulation. Genetics. 2005; 169(4):1859–71. [PubMed: 15695358]

45. Schneider KR, Smith RL, O'Shea EK. Phosphate-regulated inactivation of the kinase PHO80-PHO85 by the CDK inhibitor PHO81. Science. 1994; 266(5182):122–6. [PubMed: 7939631]

46. O'Neill EM, Kaffman A, Jolly ER, O'Shea EK. Regulation of PHO4 nuclear localization by the PHO80-PHO85 cyclin-CDK complex. Science. 1996; 271(5246):209–12. [PubMed: 8539622]

47. Carroll AS, Bishop AC, DeRisi JL, Shokat KM, O'Shea EK. Chemical inhibition of the Pho85 cyclin-dependent kinase reveals a role in the environmental stress response. Proc Natl Acad Sci U S A. 2001; 98(22):12578–83. [PubMed: 11675494]

48. Bantscheff M, Schirle M, Sweetman G, Rick J, Kuster B. Quantitative mass spectrometry in proteomics: a critical review. Anal Bioanal Chem. 2007; 389(4):1017–31. [PubMed: 17668192]

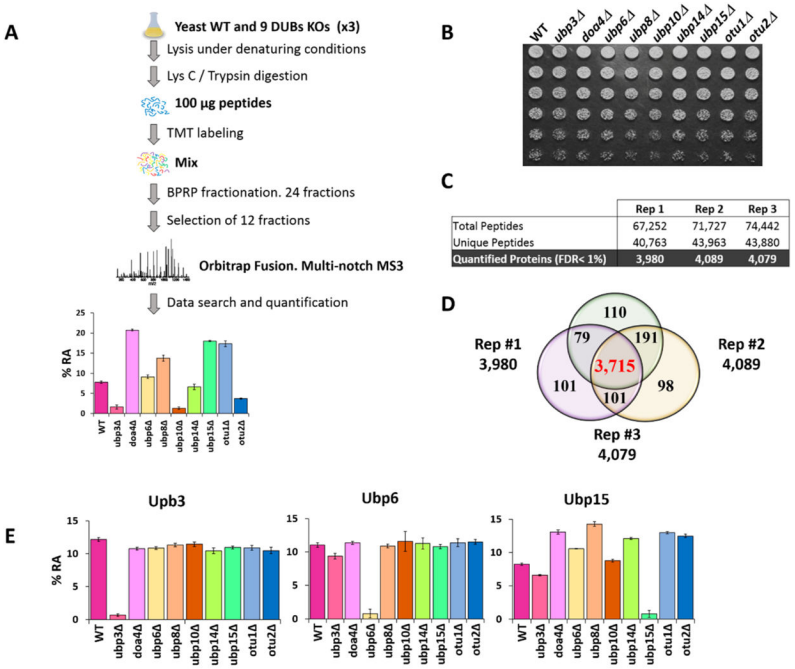

Figure 1.

Proteomic analysis of nine yeast deletion strains in triplicate. (A) Workflow overview of the MS protein analysis of nine DUB deletions and wild type strains grown in biological triplicates. (B) Growth ability in YPD of the nine DUBs deletions compared to a wild type strain. Cells (3×10^4) were spotted in the first raw and 1/3 serial dilutions were made for successive dilutions. (C) Table summarizing peptide and protein quantification for the three biological replicates. Proteins were collapsed to a final protein-level FDR < 1%. (D) Venn diagram representing quantified proteins for each experiment. A total of 3715 proteins were quantified in triplicate. (E) Examples illustrating the expected loss of deleted proteins. Data shown are means with error bars as one standard deviation ($n = 3$).

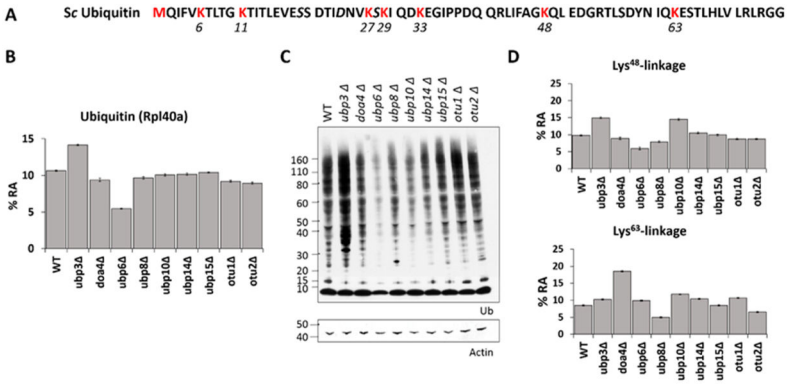

Figure 2.

Effect of nine individual DUB deletions on the total ubiquitin pool. (A) Sequence of the 76-amino-acid ubiquitin polypeptide encoded in *Saccharomyces cerevisiae*. Conjugation of multiple ubiquitin moieties can take place at seven different lysine residues (Lys^{6}, Lys^{11}, Lys^{27}, Lys^{29}, Lys^{33}, Lys^{48}, and Lys^{63}) as well as the methionine at the N-termini (all highlighted in red). (B) Relative abundance of the ubiquitin-ribosomal 60S subunit L40A fusion protein in all ten samples and the standard deviation of their mean. (C) Whole cell lysates of WT and nine DUBs deletion strains were immunobloted against ubiquitin. Equal loading was confirmed by stripping the immunoblot and reprobing for actin. (D) Lys^{48} and Lys^{63}-ubiquitin linkages were quantified in triplicate across all samples and normalized against total ubiquitin pools.

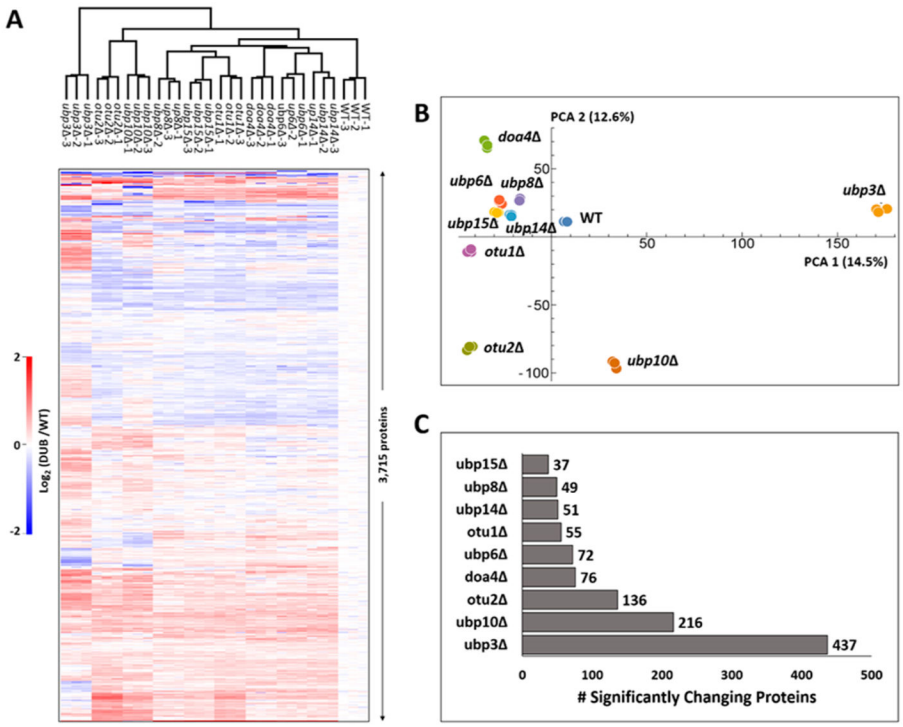

Figure 3.

Overview of protein expression differences in the yeast strains. (A) Heatmap of the 10 DUB deletion proteomes in triplicate. Protein abundance is shown as the Log2 ratio between each sample with respect to the average of reference sample (WT). (B) Principal component analysis of the relative protein abundances of all 30 values. Total explained variance of each principal component is shown in parentheses. (C) Number of significantly changing proteins in each deletion strain compared to wild type levels (adjusted *p*-value <0.01 and fold-change >1.5).

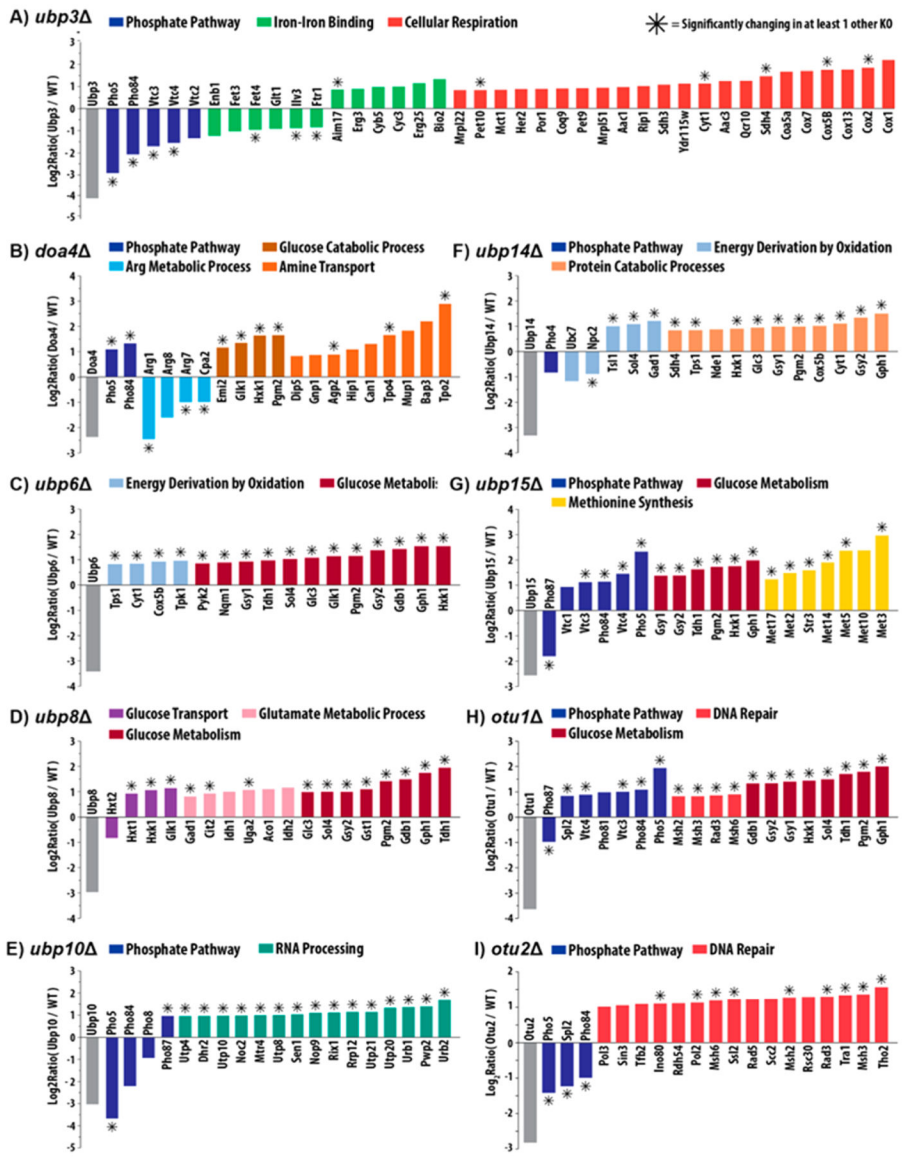

Figure 4.

Effect of individual DUBs deletions on protein abundances. Proteins with statistically significant differences in abundance (adjusted *p*-value <0.01) are represented for each DUB deletion strain. Genes are annotated in different colors based on their membership in the Biological Processes category in Gene Ontology. Genes that changed significantly in more than one DUB KO are labeled with an asterisk.

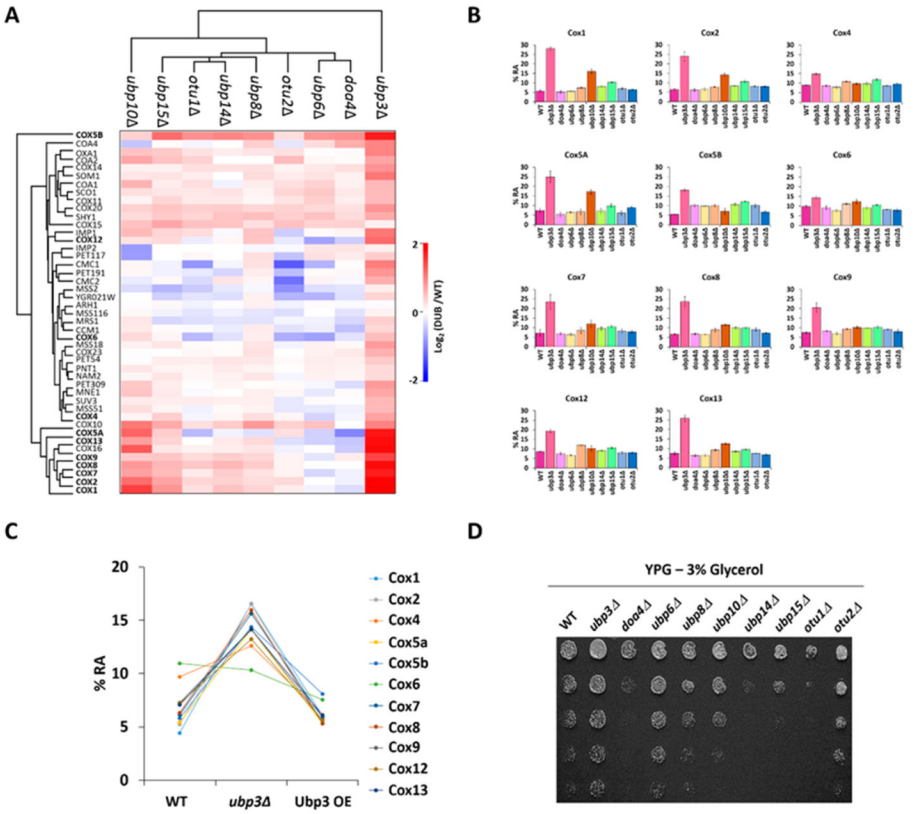

Figure 5.

UBP3 affects protein expression of many members of the COX complex. (A) Heatmap of all quantified COX subunits (bold) and their assembly factors. (B) Relative abundance of all COX subunits (mean ± SD). (C) Expression of COX subunits was decreased to wild type levels upon Ubp3 overexpression (Ubp3 OE). (D) Ability of wild type and nine DUB deletions to rescue growth defects conferred by respiratory impairment (YPGlycerol -3%). Cells (3×10^4) were spotted in the first raw, and 1/2 serial dilutions were made for successive columns.

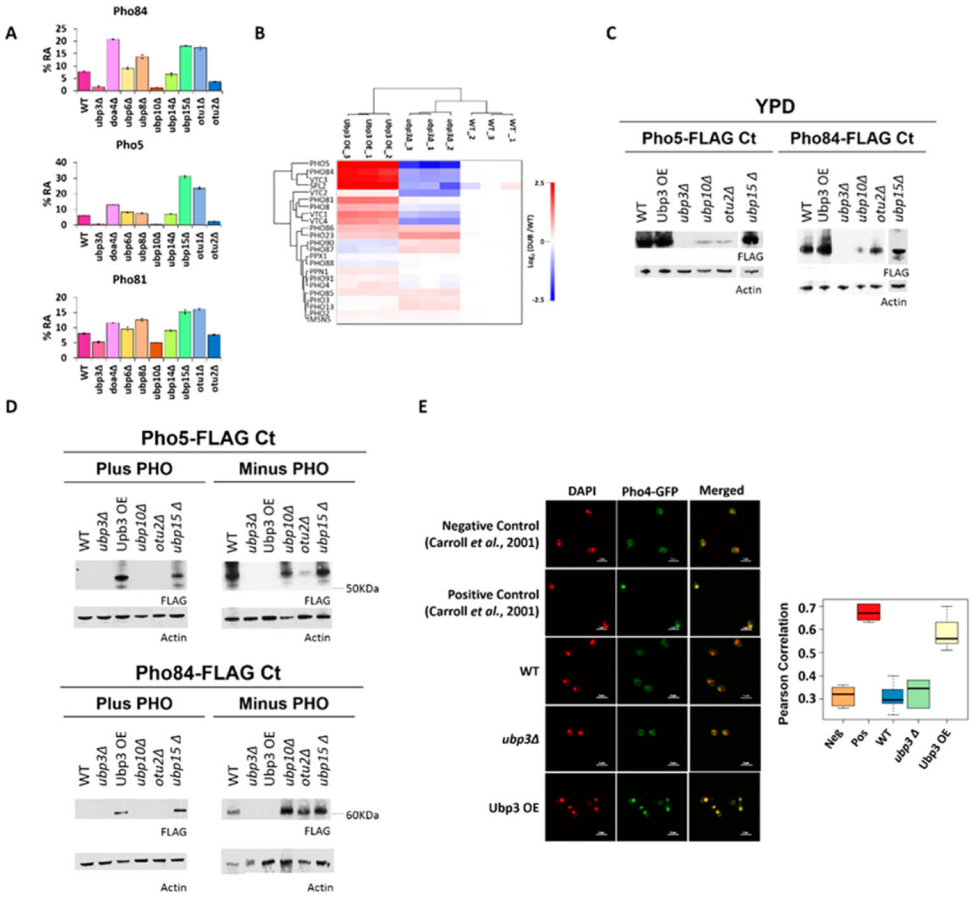

Figure 6.

DUB deletion affects the inorganic phosphate pathway. (A) Relative changes in expression for some components of the PHO pathway (mean ± SD). (B) Heatmap showing protein changes in the PHO pathway comparing triplicates of wild type, *ubp3*Δ, and Ubp3 overexpression (Ubp3 OE). Changes are expressed as Log2 ratios to mean of wild type levels. (C) C-termini tagged Pho5-FLAG (left) and Pho84-FLAG (right) expression in different mutants grown in YPD were monitored by immunoblot analysis. Actin was used as loading control. (D) Amount of Pho5-FLAG (top) and Pho84-FLAG (bottom) in the presence and absence of inorganic phosphate was examined by immunoblotting in the indicated strains. For equal loading of the samples, membranes were stripped and reprobed with actin antibody. (E) Cellular localization of Pho4 fused to GFP was monitored by immunofluorescence in WT, *ubp3*Δ, and Ubp3 OE cells. Controls as described by Carroll et al. were used as a benchmark (top). Pearson correlation of the colocalization signal of at least 100 cells per condition is shown in a box plot (bottom).